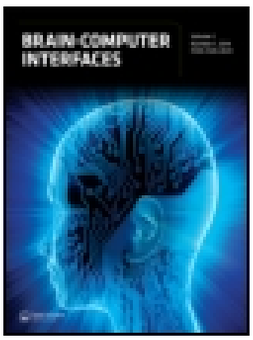

Brain-Computer Interfaces

ISSN: 2326-263X (Print) 2326-2621 (Online) Journal homepage: http://www.tandfonline.com/loi/tbci20

Depth electrode neurofeedback with a virtual reality interface

Hagar Grazya Yamin, Tomer Gazit, Natalia Tchemodanov, Gal Raz , Gilan Jackont, Fred Charles, Itzhak Fried, Talma Hendler & Marc Cavazza

To cite this article: Hagar Grazya Yamin, Tomer Gazit, Natalia Tchemodanov, Gal Raz , Gilan Jackont, Fred Charles, Itzhak Fried, Talma Hendler & Marc Cavazza (2017): Depth electrode neurofeedback with a virtual reality interface, Brain-Computer Interfaces

To link to this article: http://dx.doi.org/10.1080/2326263X.2017.1338008

Published online: 21 Jun 2017.

BRAIN–COMPUTER INTERFACES, 2017
https://doi.org/10.1080/2326263X.2017.1338008

Taylor & Francis
Taylor & Francis Group

Depth electrode neurofeedback with a virtual reality interface

Hagar Grazya Yamin[a], Tomer Gazit[a], Natalia Tchemodanov[b], Gal Raz[a], Gilan Jackont[a], Fred Charles[c], Itzhak Fried[b,d], Talma Hendler[a] and Marc Cavazza[e]

[a]Center for Brain Functions, Tel Aviv Sourasky Medical Center, Tel Aviv, Israel; [b]Department of Neurosurgery, David Geffen School of Medicine and Semel Institute for Neuroscience and Human Behavior, University of California Los Angeles, Los Angeles, CA, USA; [c]Department of Creative Technology, Faculty of Science and Technology, Bournemouth University, Poole, United Kingdom; [d]Functional Neurosurgery Unit, Tel-Aviv Medical Center and Sackler School of Medicine, Tel-Aviv University, Tel-Aviv, Israel; [e]School of Engineering and Digital Arts, University of Kent, Canterbury, United Kingdom

ABSTRACT

Invasive brain–computer interfaces (BCI) provide better signal quality in terms of spatial localization, frequencies and signal/noise ratio, in addition to giving access to deep brain regions that play important roles in cognitive or affective processes. Despite some anecdotal attempts, little work has explored the possibility of integrating such BCI input into more sophisticated interactive systems like those which can be developed with game engines. In this article, we integrated an amygdala depth electrode recorder with a virtual environment controlling a virtual crowd. Subjects were asked to down regulate their amygdala using the level of unrest in the virtual room as feedback on how successful they were. We report early results which suggest that users adapt very easily to this paradigm and that the timing and fluctuations of amygdala activity during self-regulation can be matched by crowd animation in the virtual room. This suggests that depth electrodes could also serve as high-performance affective interfaces, notwithstanding their strictly limited availability, justified on medical grounds only.

ARTICLE HISTORY
Received 30 July 2016
Accepted 8 May 2017

KEYWORDS
Brain–computer interface (BCI); neurofeedback (NF); electroencephalogram (EEG); intracranial depth electrodes

SUBJECT CLASSIFICATION CODES
Application development and evaluation; neurosurgical approaches and methods, affective computing; signal acquisition: EEG (other)

Introduction

With the development of brain–computer interfaces (BCI) as an interdisciplinary endeavor ranging from neural engineering to user interface technology [1], there has been a growing interest in invasive BCI developed in clinical settings, to gain knowledge on some fundamental BCI problems, and more speculatively, develop user interfaces around invasive BCI. Invasive systems are implemented for strict medical indications, primarily the monitoring and presurgical evaluation of medically intractable epilepsy [2]. The two main invasive approaches are electrocorticography (ECoG, [2–4]) where intracranial electrodes are placed at the surface of the cerebral cortex, and depth electrodes which are inserted inside inaccessible regions, for instance to monitor and control temporal epilepsy [5]. Compared to EEG electrodes, invasive recordings offer a better spatial resolution, the ability to capture high EEG frequencies with fewer artifacts and, in the case of depth electrodes, an even greater spatial resolution, and the ability to access deep regions such as the amygdala and hippocampus, which play important roles in cognitive and affective processing. In this article, we explore the development of a depth electrode BCI using a neurofeedback (NF) paradigm, in which users are asked to down-regulate their amygdala (gamma band) activity to control the behavior of a virtual environment populated by a small crowd of virtual characters. This system was originally developed to improve engagement for patients having to test the recording ability of their implanted depth electrodes, and we report here early results on its use in two patients to illustrate the properties of depth electrodes BCI and the end-to-end integration in a virtual environment based on the Unreal Development Kit (UDK™) engine.

Previous and related work

Although the literature on invasive BCI primarily addresses assistive technology for motor impaired patients, several authors have reported experiments in which users were able to control other applications, in particular computer

CONTACT Hagar Grazya Yamin yaminhagar@yahoo.com

games, as an illustration of quality and controllability of the signal. Breshears et al. [6] have used ECoG as an interface to a version of the popular Space Invader game in which a young patient would control one-dimensional lateral movement of the base spaceship that would fire autonomously. The same group had previously demonstrated the possibility of controlling a cursor in two dimensions with success rates of 53–73% [7]. Previous BCI making use of depth electrodes include Krusienski and Shih [8] who have adapted the P300 spelling paradigm for use with a depth electrode, describing its use by one subject with a hippocampal depth electrode [9]. Lachaux et al. [10] have reported the use of depth electrodes for neurofeedback, using the direct visualization of plotted cortical activity as a visual feedback channel. The same team was the first to use this paradigm with a bespoke game called 'Brain Ball' in which subjects would control the position of a ball on the screen by self-initiated gamma power (triggered by voluntarily engaging in mental calculation). In terms of signal mapping, the instantaneous position of the ball was updated in real-time according to a linear transformation of the instantaneous change in gamma power from the parietal depth electrode [11].

Overall, this article is the first to combine depth electrodes in a neurofeedback context with a realistic, real-time game-like interface developed using the Unreal Development Kit (UDK^{TM}) engine. In addition, we depart from direct physical control of motion direction or position (spaceship, ball) to consider more abstract concepts of mental/affective state regulation for which the 3-D interface is primarily a metaphor. Importantly, this metaphor still establishes continuity between the cognitive strategy and the controlled game, as the user aims at simultaneously activating/deactivating the target region and agitating/relaxing the 'Waiting Room'. This contrasts, for instance, with the use of cognitive tasks such as mental calculation to control the position of the ball in Brain Ball [12]. Like previous work, we report on isolated numbers of patients (here two patients), so the findings are to be interpreted in the context of previous literature and the description of fundamental phenomena associated with neural activity, and claim no statistical validity.

System overview

We developed a user interface concept to support NF called the 'Waiting Room' (WR), which is a virtual environment populated by animated characters (see Figure 1). One frequently observed issue in NF is that the usability of traditional feedback signals (e.g., gages and thermometers) is often limited, for two reasons. The first one is the lack of user engagement in a context which is seen as too close to an assessment or an experiment. By contrast, embedding feedback into a task-based application or a game is known to improve engagement [2]. The second one is that full synchronous coupling between the measured BCI signal and the visual signal tends to feedback all oscillations and inherent instability related to the effortful component of neurofeedback, which can lead to loss of focus, or 'catastrophic' reactions when the user cannot sustain their neurofeedback effort. This is the case in particular with high frequency signals derived from EEG: resampling through moving averages smoothens variations, but at the cost of delays and impact on variation ranges.

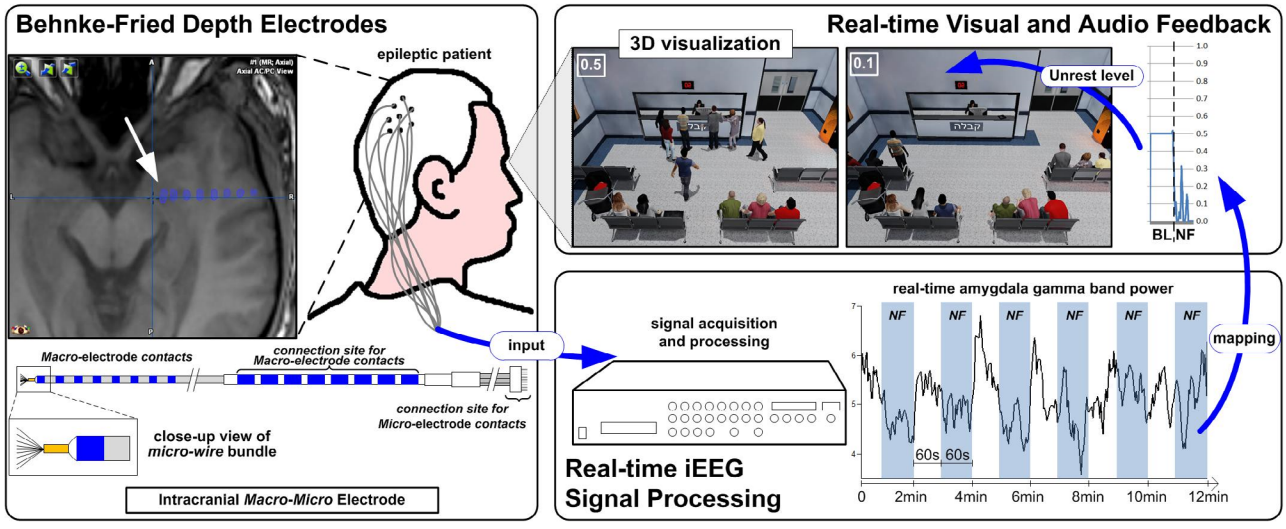

Figure 1. System Overview and Experimental Setting. The user, implanted with Behnke–Fried depth electrode [19], is instructed to appease the situation in the real-time 3-D visualization of the 'Waiting Room'. Neurofeedback is based on the input of gamma band amygdala iEEG power. iEEG is recorded using Neuroport (Blackrock microsystems). The user is expected to lower the level of unrest in the 'Waiting Room' by down-regulating her amygdala activity. The real-time amygdala gamma band power is plotted during several short NF trials, where the NF epochs (in blue) must show lower values than during the Baseline epochs (in white).

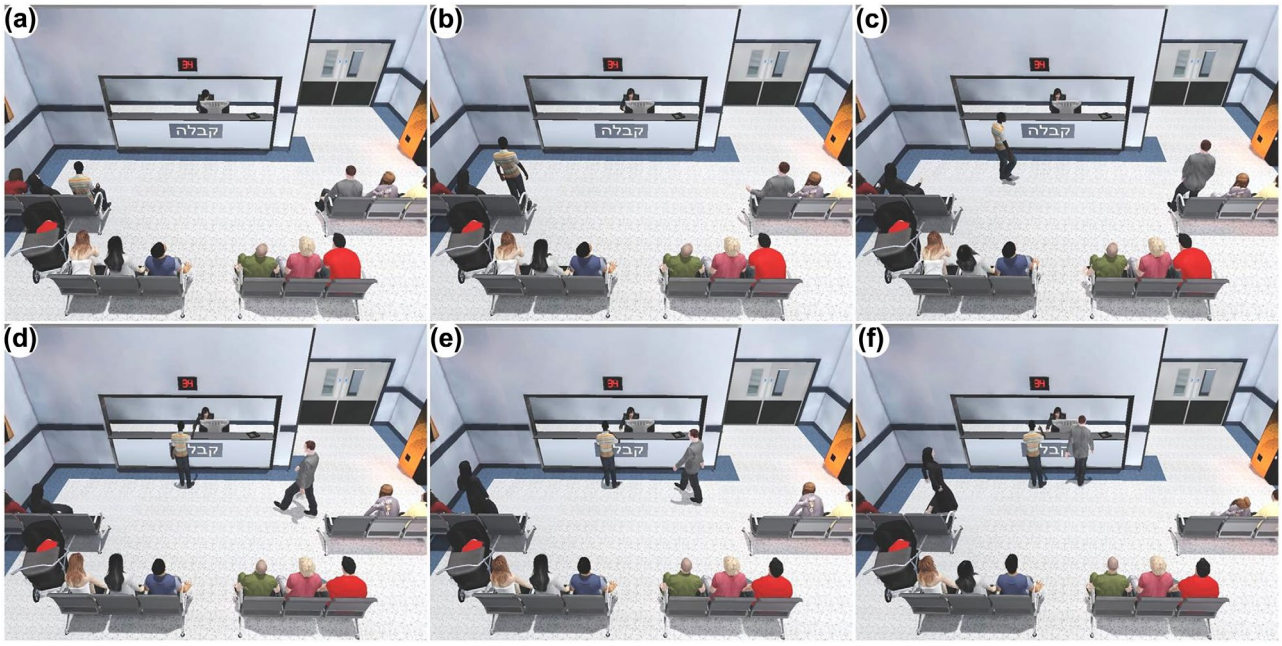

Figure 2. Characters standing up from their seats and walking to the reception desk.

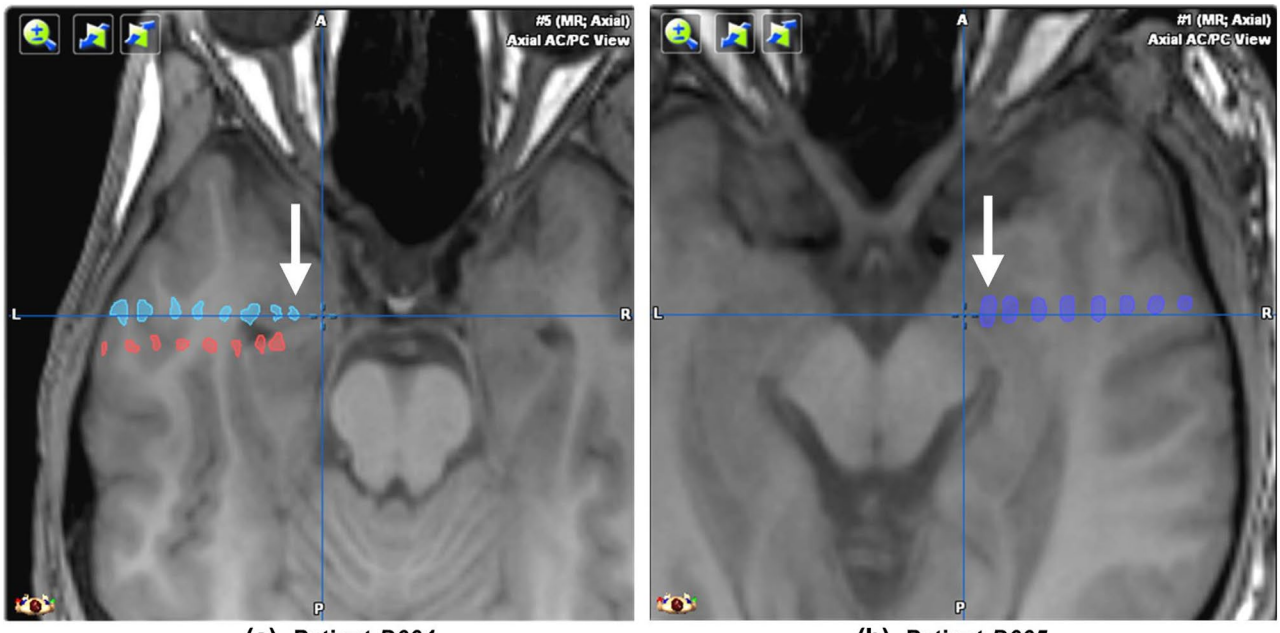

(a) Patient *D004* **(b) Patient *D005***

Figure 3. Arrows represent the deepest macro contact located in the left amygdala of patient D004 (a) and in the right amygdala of patient D005 (b). The unmarked bulbs represent the location of the rest of the macro contacts on the same electrode (light blue in (a) and purple in (b)) or at a nearby electrode (red bulbs in (a)).

A more appropriate feedback interface would both have a realistic (semantic) outlook and support some kind of signal integration that would sustain the user's neurofeedback cognitive efforts, by canceling transient dips in activation towards the threshold (regardless of the position of the threshold with respect to the baseline). The WR is designed to meet these requirements, and uses a crowd of virtual characters as a metaphor for arousal (see Figure 2). The characters can evolve between two states: one resting state, in which they are sat waiting to be called; and one agitated state, in which they move to the front desk to complain about waiting times. The ratio between the characters standing and sitting (N_{stand}/N_{sit}) at the desk defines a level of 'unrest', which is used as the target variable for

Table 1. Total number of electrodes and the positioning of the target amygdala macro electrode for the two subjects.

Patient ID	Total number of electrodes	Amygdala macro electrode MNI
D004	6	Left: x = −24, y = −4, z = −24 Right: x = 24, y = −6, z = −29 (located at the border with the hippocampus)
D005	10	Left: x = −24, y = −8, z = −26 (located at the border with the hippocampus) Right: x =24, y = −8, z = −17

BCI signal mapping. The level of activation for the amygdala is translated into a level of unrest, which is updated in the WR through a set of discrete transitions during which additional characters stand up and move towards the front desk. It is this realistic simulation of characters motion that dampens the BCI signal fluctuation, because the time required for characters to move across the room prevents drastic changes in either populations (waiting or standing).

Methods

Apparatus

We used Behnke–Fried depth electrodes (Ad-Tech medical instruments, USA; see Figure 1) [1,5]. Each electrode has eight platinum-coated macro contacts (1.6 mm diameter, separated by 5 mm), and eight platinum-iridium micro contacts (seven recording and one reference electrode) located at the tip of each electrode (38 μm diameter). The micro contacts are capable of recording single units, whereas the macrowires record activity of a wider volume referenced here as iEEG. Because the gamma band activity collected by the microwires was more prone to noise, we used macro contact data for neurofeedback purposes.

Subjects

Two adult patients recruited at the authors' institution (D004: male, 23 years old; and D005: male, 40 years old) with intractable epilepsy were implanted with depth electrodes to localize the epileptic focus for possible subsequent resection. Patients were stereotactically implanted with six and ten depth electrodes from a lateral orthogonal approach aiming at targets selected using clinical criteria. Following implantation, patients remained between one and two weeks hospitalized for monitoring (subject D004 10 days, subject D005 14 days). All patients provided informed consent. All studies conformed to the guidelines of the authors' institution. All patients underwent intracerebral EEG recordings using stereotactically implanted depth electrodes [12,13].

The macro contacts used for neurofeedback are in most cases in the target region (AM); in some cases they are in the boundary with the hippocampus; it is summarized in Table 1. In patient D004 and the first session of D005, the feedback was bilateral, the feedback of the second session of D005 was taken from the right amygdala.

We localized electrodes by performing computed tomography scans after implant; aligning the computed tomography images with pre-implant MRIs and then labeling the region of each electrode according to anatomical landmarks (see Figure 3).

The placement of electrodes is based solely on the data obtained from scalp EEG, imaging and other tests undergone by the patient. Likewise, the length of time the patient remains implanted is determined only by the requirement to 'capture' sufficient seizures on EEG to determine the seizure onset zone.

Sampling and signal acquisition

The online interaction between the Neuroport system and the MatLab file controlling the WR was done using *cbmex* platform, a set of MatLab functions provided by Blackrock Microsystem for online communication, with the data collected through the neural signal processors.

The system amplifier receives signals directly from the electrodes through a headstage or the patient cable. The sampled signal (up to 30 kHz) is amplified, analog filtered (1st-order high-pass at 0.3 Hz and 3rd-order low-pass at 7,500 Hz) and digitized (16-bits at 250 nV resolution) and then is transmitted to the NSP via a fiber optic link. The analog filter allows for the low-frequency field potentials as well as the higher frequency spike signals to be recorded. A later stage digital filtering will allow these two signals to be separated (NeuroPort user's manual, Blackrock Microsystems). Here we used the low frequency field potentials, the signals were digitally sampled at 2 kHz, and bandpass filtered between 0.3 and 500 Hz (Neuroport, Blackrock Microsystems, USA). All macro contacts were referenced to a scalp electrode (Pz).

Neurofeedback setting: the Waiting Room

The visual neurofeedback signal, which is the variable to be controlled by the user, corresponds to the unrest level of the WR. The WR layout makes the unrest state immediately visible to the user through the number of characters

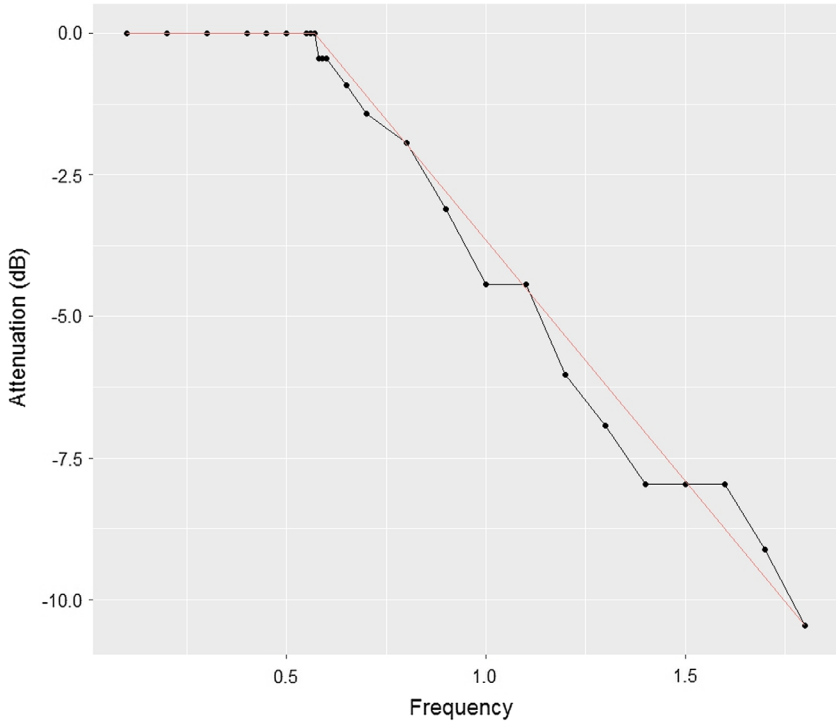

Figure 4. Signal damping properties of the Waiting Room, plotted with simulated input signals (see Figure 5). The 'lowpass' filtering effect limits rapid fluctuation of unrest levels during neurofeedback (see text for details).

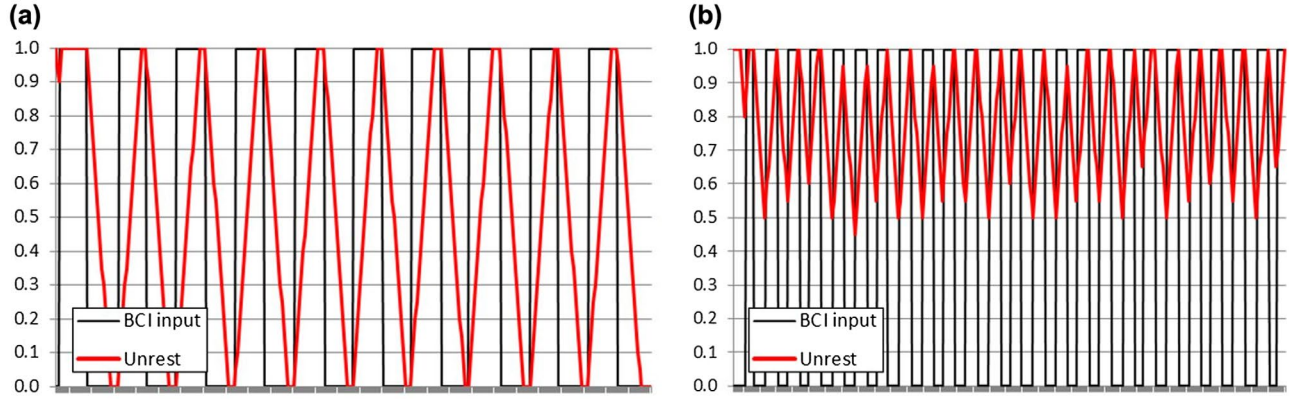

Figure 5. Damping properties of BCI signal input by the WR at various frequencies obtained through input signal simulation. The spatial layout and updating mode of the WR damps input signal fluctuations, which is meant to facilitate subjects' NF effort, by making transient fluctuations less visible. BCI input consists of a target unrest level determined by statistical testing of the iEEG NF signal against a resting epoch baseline. Actual WR unrest closely follows variations at low frequencies (Figure 5a) while it fluctuates around an average higher value at higher frequencies (Figure 5b). These damping properties are also visible on actual signals on Figure 9.

standing at the desk. To preserve the visual realism of the setting, transitions between levels of unrest are represented through real-time animations showing characters moving from one location (front desk) to the other (sitting area). The flow of characters, from or towards the desk, also gives a clear trend on whether the user succeeds in sustaining the neurofeedback signal, while damping the BCI input signal fluctuations (see below).

It is possible to generate initial configurations at any given unrest state: for instance, when the user is tasked with 'calming down' the WR, the initial distribution corresponds to an unrest value of [0.5–1.0] for which a significant fraction of characters are in their standing state. This situation makes it possible to give feedback to the user whatever the variation of her BCI input signal, which is important in the early stages of a neurofeedback epoch.

The WR unifies an engaging task, which is a good visual metaphor for arousal, with an empirical mechanism to damp neurofeedback signal fluctuations, potentially facilitating adaptation to the neurofeedback task with minimal training.

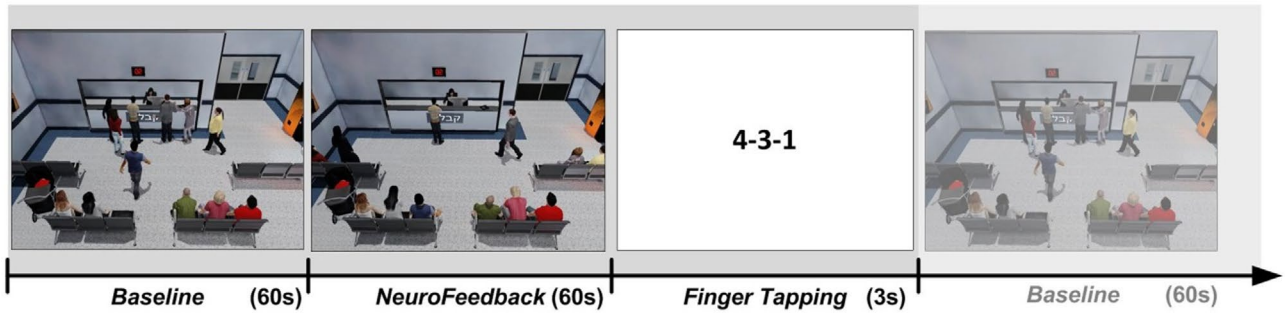

Figure 6. Block design. Each of the sessions included a baseline epoch (BL) of passive viewing of the Waiting Room environment for 60 s, for which the unrest level was set to 0.5; an active neurofeedback epoch (NF) for 60 s; and a finger tapping epoch for 3 s, to restore the baseline.

In order to characterize these signal damping properties, we have performed an empirical evaluation using generated square signals simulating BCI input to the WR, which consists of a target unrest level to be visualized in the WR.

We have generated square signals in a frequency range corresponding to expected fluctuations of the BCI input signals, i.e. [0.1–2 Hz], with an amplitude varying across the full [0,1] interval of unrest values. At each frequency, we have recorded the WR response in terms of oscillation of the actual unrest value and have computed signal attenuation in dB using maximum amplitude for both input (simulated square target unrest) and output (actual unrest) signals. Results from this simulation are plotted on Figure 4. The simulated input signal varies over the amplitude of the normalized input signal (iEEG) rather than 'unrest values', which are automatically derived from it. The attenuation is computed from the initial unrest value corresponding to the simulated input rather than the updated one. These results confirm that the WR is acting as a kind of 'lowpass filter' where amplitude starts decreasing for frequencies > 0.6 Hz and with an attenuation level of –8.5 dB/Hz, effectively limiting sudden variations of the BCI input signal (here, target unrest).

Figure 5 illustrates more specifically the lowpass filtering behavior at two simulated frequencies. On Figure 5a, for low fluctuations, the WR response closely follows the variations of the input signal. However, at higher frequencies (Figure 5b), physical state transitions cannot be completed within the time range of fluctuations, because the next update cycle is triggered before some characters have reached their previous target state due to the time required to travel through the environment, even preventing some characters from changing state altogether. This results in the WR unrest fluctuating around an average value.

Neurofeedback

Each of the NF sessions included four to eight baseline (BL) epochs of passive viewing of the WR environment (60 s each) following an equivalent number of active neurofeedback (NF) epochs (60 s each) (see details of protocol design in Figure 6). Between blocks, a 3 s finger tapping block was introduced; we have set the finger tapping to the shortest possible latency, as analysis of preliminary data revealed that the use of finger tapping washout period does not facilitate the execution of the paradigm. The participants were instructed to 'appease the waiting room using their brain activity'. No preferred cognitive strategy was specified for NF, to avoid influencing subject's down-regulation.

The NF probe was the energy in the gamma band (25–35 Hz and 65–85 Hz), the band around 50 Hz was removed to avoid line noise. The probe was calculated every 1 s using Welch power spectrum estimation method with eight time windows with 50% overlap (*pwelch* Matlab function). The calculated values were averaged every 3 s.

Higher gamma band activity is shown in animal models of chronic stress [14] and in humans exposed to fearful stimuli [15,16]. The study of Gaona et al. [17] suggested the specificity of different sub-bands across the 60–500 Hz range to various cognitive tasks [7]. Gamma oscillations have been associated with a wide range of cognitive processes including perception, attention and memory [2,18]. In addition, Jerbi et al. [12] used high-gamma frequency (60–140 Hz) for their depth electrode BCI based on cognitive tasks.

In the BL, blocks the probe values were used to construct a distribution of gamma power, to which the probe values in the NF blocks will be compared. NF probe values were compared to the BL values immediately preceding it. During BL, outliers were treated as follow: values exceeding *median + 10SD* of the 90 first percentiles of the BL probe was replaced with the median. Then the median and standard deviation (SD) of the BL probe values were recalculated and a normal cumulative distribution function (*normCDF*) with this value was estimated. In the NF, blocks probe values were compared to the *normCDF*, if the probability to receive the NF value or higher in the

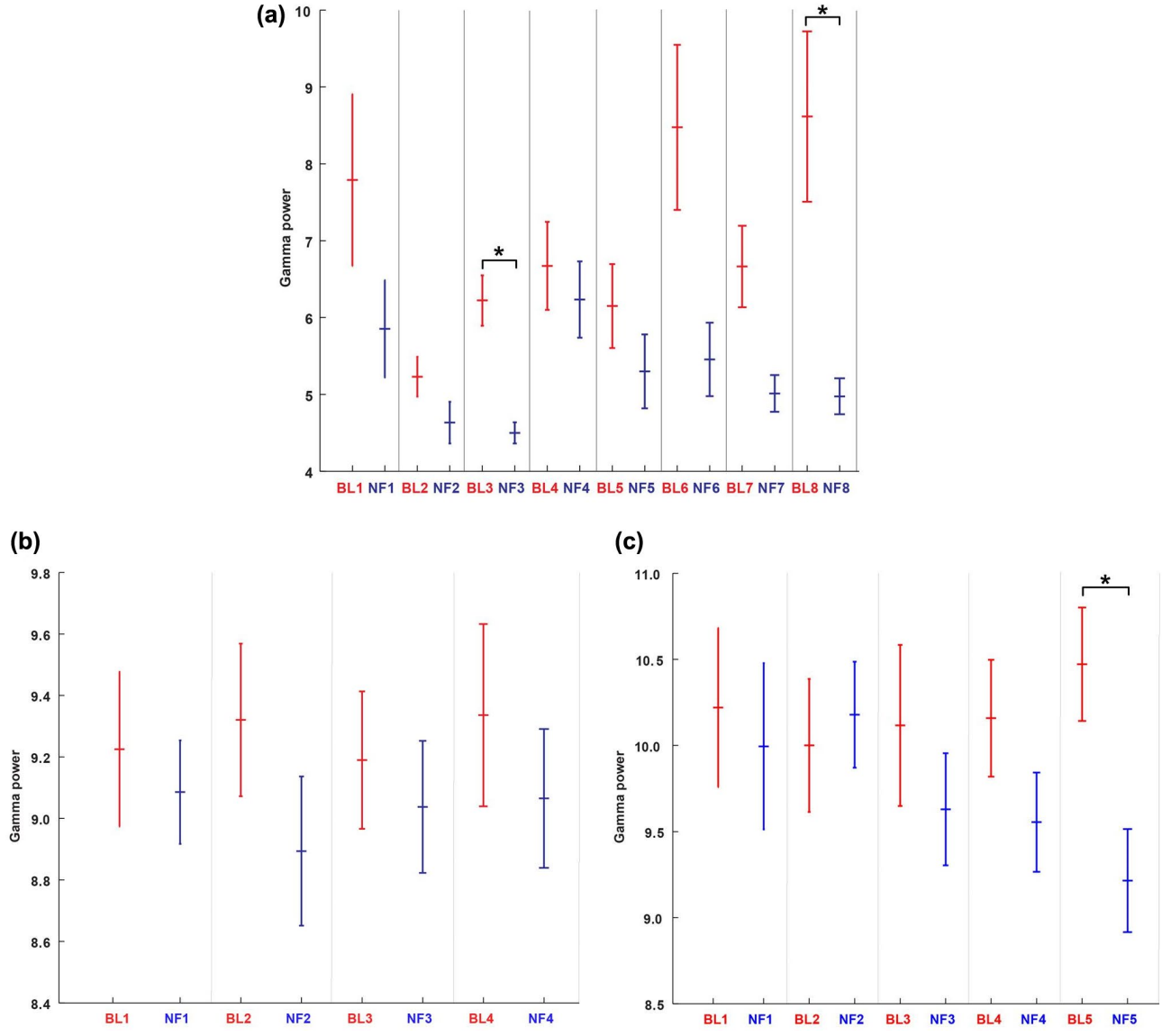

Figure 7. The results presented (from patient D004 in (a); from patient D005 in (b) and (c)) show the average ± SEM of values of gamma power for the baseline (labeled BL#) and the neurofeedback (labeled NF#) epochs. In (a), two trials show a significant down-regulation, marked by *. Blue bars (NF) show a trend in down-regulation, although only one trial BL5-NF5 (in (c)) shows a significant down-regulation.

BL was in the range 0.25 to 0.75, the WR received 0.5, i.e. no change in the state of the room. For probabilities exceeding those values, the WR received the probability itself and the WR was changed accordingly. This was done in order to reinforce major changes in the activity; i.e. minor changes around the median activity in the BL did not receive any feedback.

Data analysis

All data analysis was performed using manually written scripts in Matlab (Mathworks, Natick, MA, USA). Before calculating the spectrogram macro contact signals were down sampled to 400 Hz, enabling spectral inference in the range 0–200 Hz (Nyquist frequency). The down sampling to 400 Hz was done by using Matlab's resample function, which applies an antialiasing FIR low pass filter to the signal and compensates for the delay introduced by the filter. Spectrograms were calculated using the welch method; parameters were selected to receive 1 Hz frequency resolution and 1 s temporal resolution. After calculating the spectrogram, a trace of the power at the different frequency bands – delta (0–4 Hz), theta (4–8 Hz), alpha (8–16 Hz), beta (16–25 Hz), gamma (25–35 Hz and 65–85 Hz) and high gamma (85–200 Hz) – was calculated by averaging the power in the specific frequency range. Each trace of different frequency band was z scored, because we were interested in the change in power and not its absolute value. From each of these traces a vector in length 2*number of blocks, in which each entry

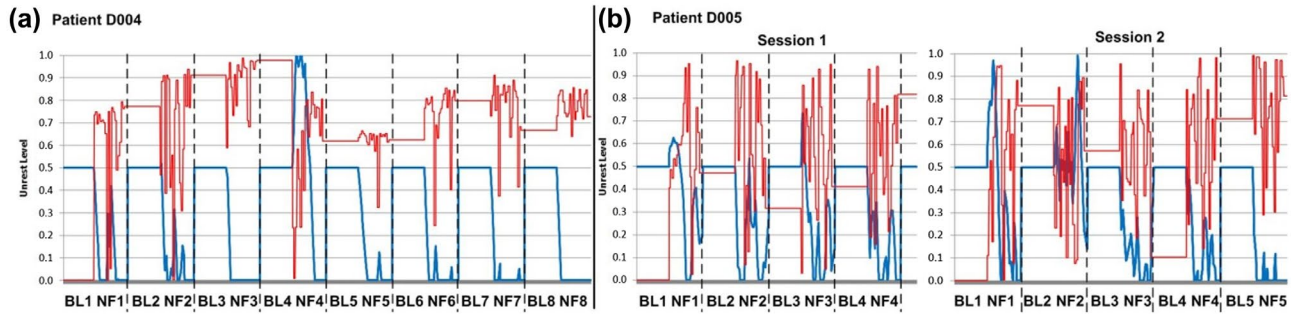

Figure 8. NF sessions showing the input (in red) and output (in blue) of the WR application for patient D004 (a) and for the two sessions from patient D005 (b). The input levels (in red) during NF are normalized to the BL probe probability as describes in the method section. Notice that the processed iEEG input levels (in red) are only relevant during NF, as in BL the unrest level of the room is predetermined, therefore the input values in the BL section are steady and does not reflect the gamma power of the macro contact.

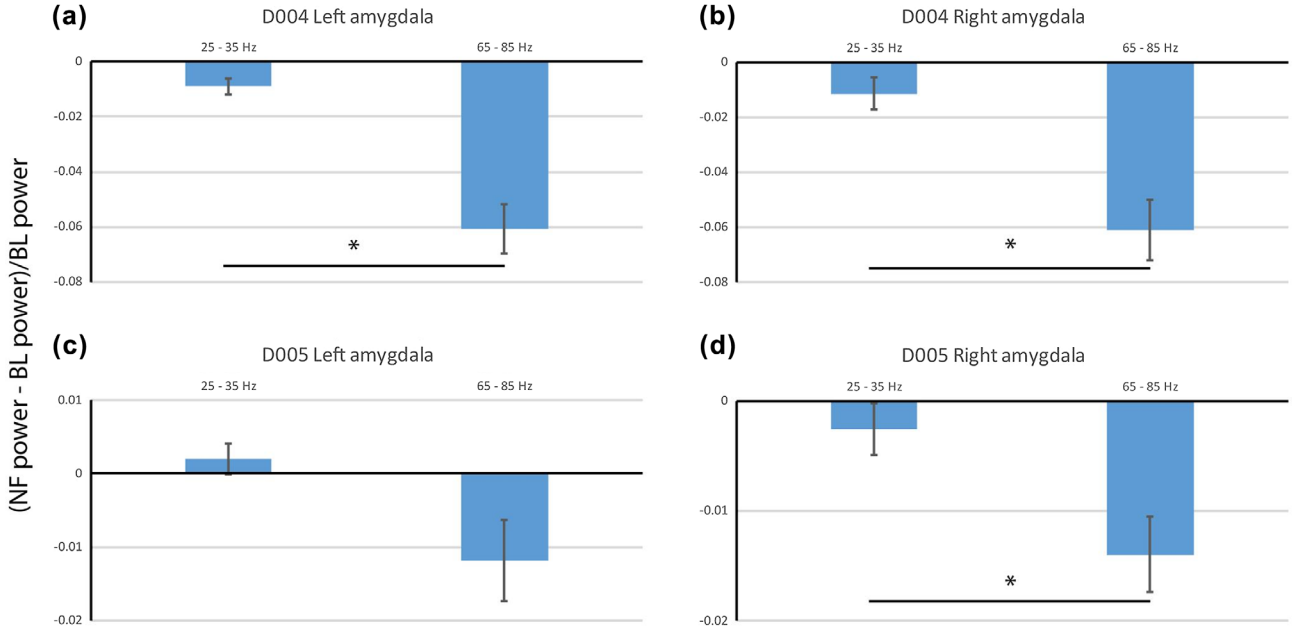

Figure 9. The down-regulation of the higher gamma band (65–85 Hz) is more prominent than the lower band (25–35 Hz). (a–d) the fraction of reduction in gamma power divided to lower and higher ranges used in the paradigm. The reduction in the higher gamma range is more prominent for both subjects, though it does not reach significance for the left amygdala of subject D005. * represents statistical significance in a paired t-test with $p < 0.05$.

represents the average power in a frequency band in a certain block was created. Each such vector represents the course of change in power along the paradigm, similar to that plotted in Figure 7.

All correlations were Pearson correlations and were calculated using Matlab's corr function.

Results

Three sessions from two patients, one from D004 (with eight BL-NF blocks) and two from D005 (with four and five BL-NF blocks), were analyzed. Figure 7 presents the average gamma power along the BL-NF blocks of the sessions, for patient D004 and patient D005. The analysis of these preliminary data suggests that participants acquired the ability to down-regulate their amygdala gamma band activity obtained by depth electrodes even with little training. A successful relaxation block was defined as a block during which amygdala gamma power values were significantly lower than those recorded in the baseline blocks (Wilcoxon signed rank test; $p < 0.05$ Bonferroni corrected for the number of blocks in a session). Success was found in 17% of the relaxation blocks. The successful blocks are marked with an asterisk in Figure 7.

A successful relaxation session was defined as a session in which the gamma power in all NF blocks pulled together was lower than the BL blocks. Two out of the three sessions were found successful: the session of D004 and the second session of D005 (Wilcoxon signed rank test; $p < 0.05$).

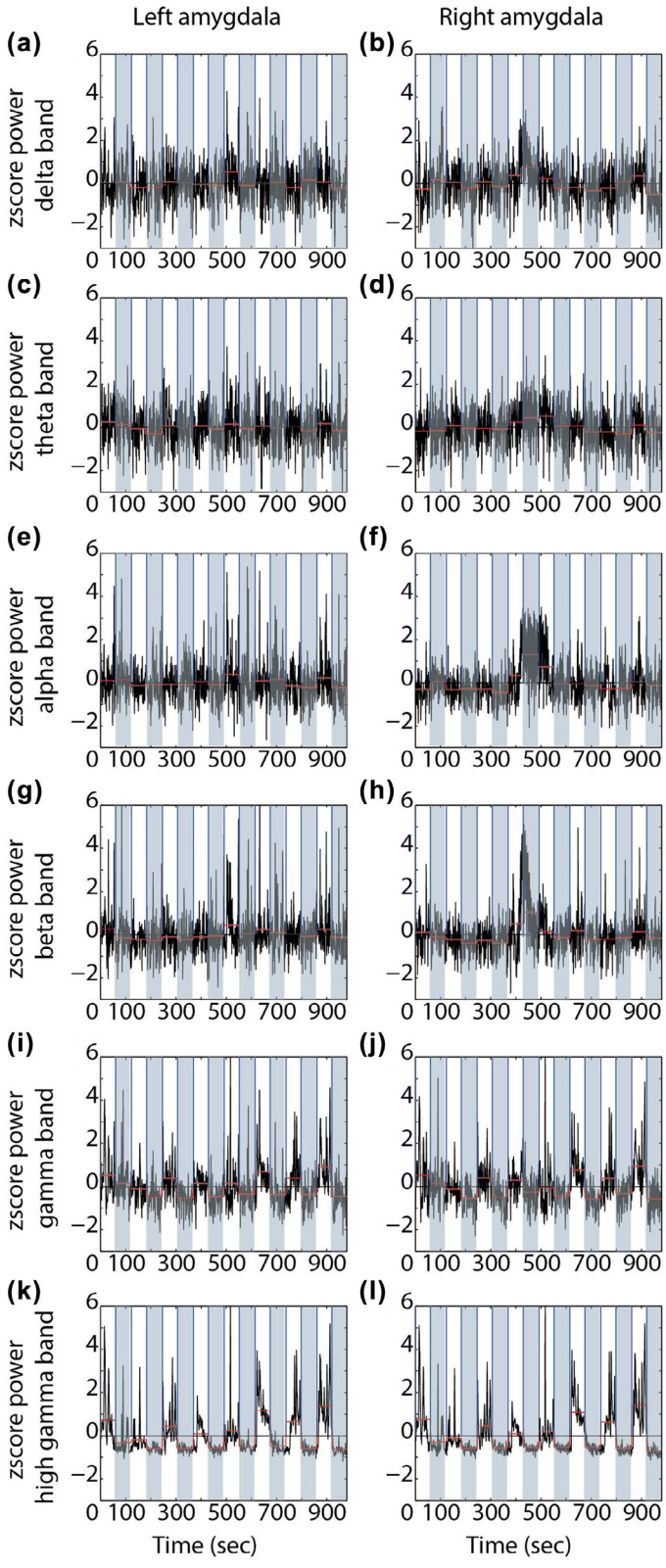

Figure 10. The modulation in power is restricted to the gamma band. The power trace (black line) and the average power in BL (white background) and NF (blue background) blocks (red line) for the right (right panel) and left (left panel) amygdala of subject D004 for the delta (a–b), theta (c–d), alpha (e–f), beta (g–h), gamma (i–j) and high gamma (k–l) bands. The reduction in mean power between BL and NF blocks is apparent in the gamma and high gamma bands.

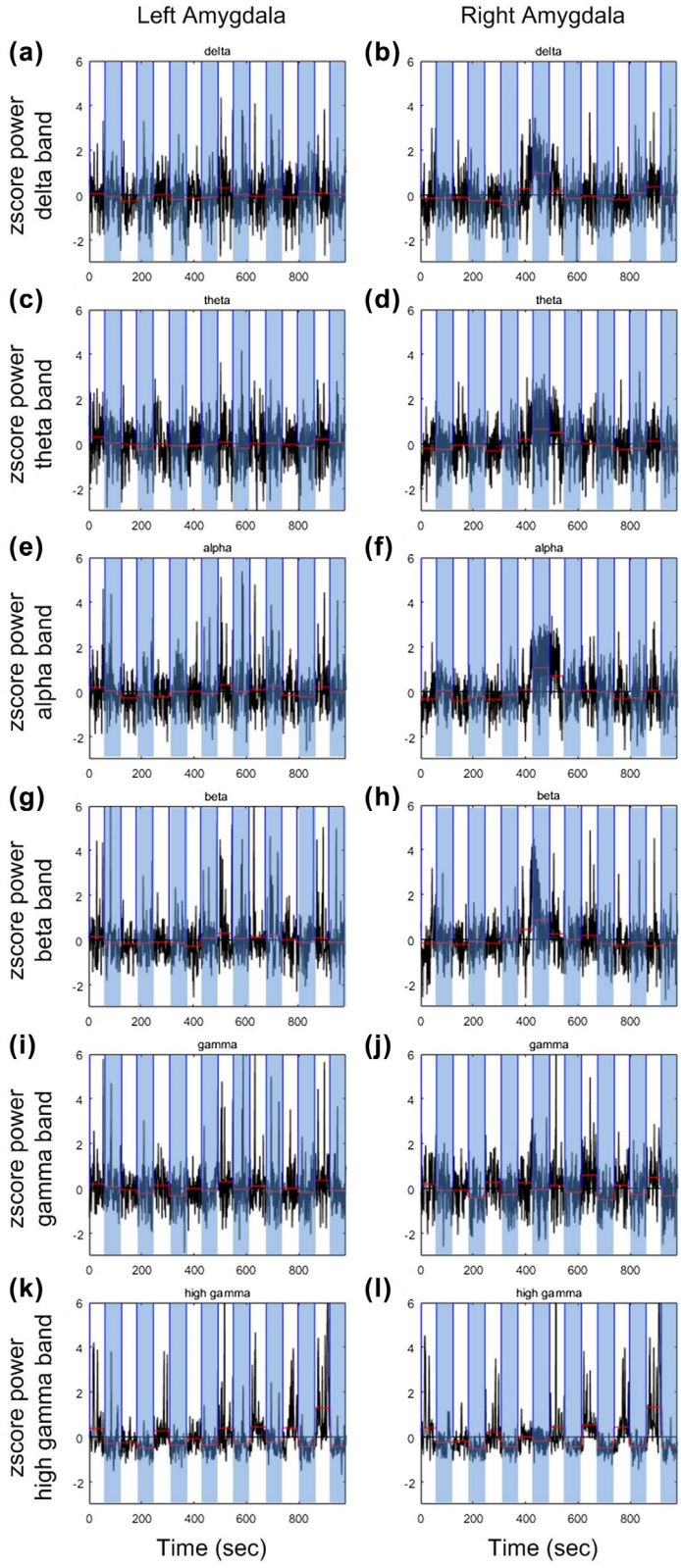

Figure 11. Inspection of the re-referenced signal in the target macro wires showing that the effect in the amygdala is maintained. The power trace (black line) and the average power in BL (white background) and NF (blue background) blocks (red line) for the right (right panel) and left (left panel) amygdala of subject D004 for the delta (a–b), theta (c–d), alpha (e–f), beta (g–h), gamma (i–j) and high gamma (k–l) bands.

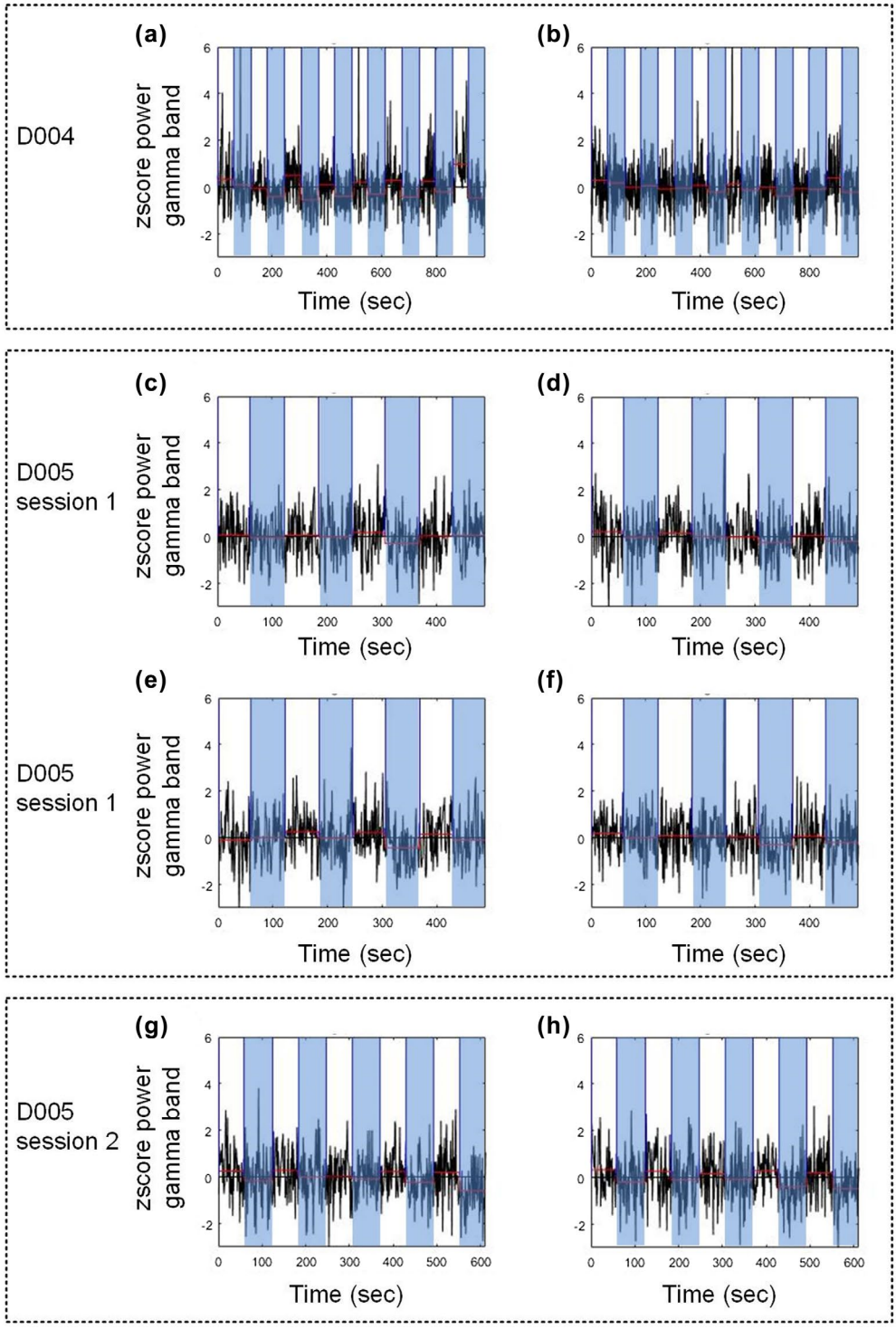

Figure 12. Subset of gamma activity from contacts correlated with the activity of the amygdala during the task, from patients D004 and D005. The power trace (black line) and the average power in BL (white background) and NF (blue background) blocks (red line) from D004: (a) left cerebral white matter; (b) right cerebral white matter; D005 session 1: (c) left hippocampus; (d) right amygdala; (e) right cerebral white matter; (f) right hippocampus; D005 session 2: (g) right amygdala; (h) right cerebral white matter.

In a post-session interview with the subjects regarding their used strategy to calm the room, D004 reported he tried to calm himself down, whereas D005 stated he mentally spoke to the crowd in the waiting room telling them to relax. The difference in strategies – one introspective and the other extrospective – might influence their success rate and the recruiting of other brain regions except the amygdala.

Figure 8 shows the variations of the unrest level (Nstand/Nsit – blue line) in the WR per BL corresponding

Table 2. Areas (macro contacts) with significant Pearson's r correlations to the target (amygdala). Correlations were calculated after re-referencing.

Subject	Macro contact location	Pearson's r Correlation
D004	Right hippocampus	0.63
D004	Right hippocampus	0.73
D004	Right hippocampus	0.73
D004	Right temporal white matter	0.55
D004	Right temporal white matter	0.61
D004	Right amygdala	0.79
D004	Right amygdala	0.74
D004	Right temporal white matter	0.76
D004	Right temporal white matter	0.77
D004	Left temporal white matter	0.58
D004	Left middle temporal gyrus	0.55
D004	Left amygdala	0.70
D004	Left temporal white matter	0.57
D004	Left temporal white matter	0.65
D004	Left temporal white matter	0.56
D004	Left middle temporal gyrus	0.52
D005 – 1	Right amygdala	0.88
D005 – 1	Right temporal white matter	0.71
D005 – 1	Right hippocampus	0.81
D005 – 1	Left hippocampus	0.85
D005 – 2	Right temporal white matter	0.94
D005 – 2	Right temporal white matter	0.80

to the input level of relative gamma power (red line). The level of unrest in the BL epoch was set to 0.5 by default and was not influenced by the gamma power.

Due to the relatively wide frequency range that we have used for feedback, we wanted to test whether the observed reduction in gamma power is similar at the entire range or is affected by the lower (25–35 Hz) or higher range (65–85 Hz). To that aim we have calculated for each subject the fraction of reduction in power between BL and the following NF block ((NF power–BL power)/BL power) in the lower and higher gamma range. Figure 9 depicts the average fraction of reduction in power in each of the frequency ranges for both the right and left amygdala of both subjects. Asterisks represent a significant difference between the bands (paired t-test, $p<0.05$). It shows that in most cases the reduction in power between BL and NF is more prominent at the higher frequency range used in the paradigm (65–85 Hz).

Figure 10 depicts the trace of the power in the common division of the EEG into frequency bands – delta (0–4 Hz), theta (4–8 Hz), alpha (8–16 Hz), beta (16–25 Hz), (gamma 25–35 Hz and 65–85 Hz) and high gamma (85–200 Hz) – in the two target macro contacts: the right and the left amygdala from subject D004. The black line is the instantaneous power calculated every 1 s (see Methods) and the red trace is the average power in a certain block (BL and NF interchangeably). It demonstrates that the change in power we observed in the gamma band is restricted to the target band or to higher frequency bands and, to a much lesser extent, to lower frequency bands. To quantify it, we have calculated the correlation between the average gamma power and the average power in all other frequency bands. The correlation was calculated between vectors in length 2*number of blocks, in which each entry represents the average power in a frequency band in a certain block (see Methods). The correlation was significant only between gamma and high gamma in the right amygdala of subject D004 ($R = 0.96$, $p < 0.0001$) and the left amygdala of subject D005 session 2 ($R = 0.86$, $p = 0.001$), and between gamma to theta and beta in the right amygdala of subject D004 ($R = 0.76$, $p = 0.001$ and $R = 0.60$, $p = 0.01$ for theta and beta respectively). To conclude, the volitional control by the subjects is restricted to the target band – gamma band or to high gamma band.

To verify that the volitional control is not due to global effects, we have re-referenced the macro wire to the global effect by subtracting from each signal the average signal that was collected simultaneously by all macro contacts. Inspection of the re-referenced signal in the target macro wires showed that the effect in the amygdala is maintained (see Figure 11). Furthermore, we have created for all other macro contact a vector representing its mean value in the gamma band (for a total of 47 in D004 and 71 and 73 macro contacts in D005 session 1 and 2 respectively – the difference in number is due to noisy contacts that were removed per session). For each electrode a vector sized 2*number of blocks was calculated, in which each entry represents the average power in a frequency band in a certain block. We than calculated the correlation between each macro contact activity and the pattern of activity in the amygdala. Figure 12 depicts a subset of gamma activity from contacts that were correlated with the activity of the amygdala during the task. Table 2. summarizes the significant Pearson correlations ($p < 0.05$); it is noticeable that only a small fraction of the contacts was correlated with the NF probe (11.5%), and that the structures correlated with it are all in the temporal lobe, which has functional connectivity to the amygdala. Thus, the volitional control of the amygdala gamma band activity was specific to cortical circuits that are functionally related to the amygdala.

Here we have presented preliminary results demonstrating that it is possible to train subjects to directly and specifically modulate their amygdala's activity using depth electrodes as a signal acquisition device. Results obtained are encouraging, in particular the relatively high success rate considering minimal training received by subjects.

Conclusions

We have presented results showing the successful use of a depth electrode BCI by two patients. For the foreseeable future, and considering the risks and side effects of depth electrodes, these systems will be restricted to patients who have received a therapeutic indication. Their use as BCI will be mostly a side effect, which distinguishes them from

BCI use to assist patients with motor impairment. From an interface technology perspective, the type of system we have presented has the potential to favor engagement in therapeutic testing phases of the iEEG, which was the initial rationale for its development. However, following previous reports [6], we can speculate that the use of BCI in a gaming context could have a positive effect on patients' morale and self-esteem, and potentially improve their acceptance of the equipment.

Overall, we have shown that it is possible to harness the power of depth electrodes to readily integrate them as BCI in a typical interactive application. In addition to the potential of VR or gaming interfaces for patient engagement, we have also reported some emergent properties of these interfaces in terms of input signal filtering. The dynamic properties of the interface related to the timing of realistic animations result in a low pass filtering that may play a role in facilitating subjects' adaptation to the neurofeedback task. Such a feature could prove of a specific interest whenever options for neurofeedback training sessions are limited, as is the case with depth electrodes. Despite the very minimal user sample, the fact that signal behavior was consistent with published observations would encourage us to think that this approach can be reproduced.

Disclosure statement

No potential conflict of interest was reported by the authors.

Funding

This work was supported by the European Union's Seventh Framework Programme for research, technological development and demonstration [grant number 602186] and by the Ministry of Science, Technology and Space [grant number 3-11170] and by the Sagol family fund.

ORCID

Gal Raz http://orcid.org/0000-0001-9032-8613
Marc Cavazza http://orcid.org/0000-0001-6113-9696

References

[1] McFarland DJ, Wolpaw JR. Brain-computer interfaces for communication and control. Commun ACM. 2011;54(5):60–66.
[2] Jayakar P, Gotman J, Harvey AS, et al. Diagnostic utility of invasive EEG for epilepsy surgery: indications, modalities, and techniques. Epilepsia. 2016;57(11):1735–1747.
[3] Jacobs J, Kahana MJ. Direct brain recordings fuel advances in cognitive electrophysiology. Trends Cogn Sci. 2010;14(4):162–171.
[4] Schalk G, Leuthardt EC. Brain-computer interfaces using electrocorticographic signals. IEEE Rev Biomed Eng. 2011;4:140–154.
[5] Engel AK, Moll CK, Fried I, et al. Invasive recordings from the human brain: clinical insights and beyond. Nat Rev Neurosci.. 2005;6(1):35–47.
[6] Breshears JD, Gaona CM, Roland JL, et al. Decoding motor signals from the pediatric cortex: implications for brain-computer interfaces in children. Pediatrics. 2001;128(1):160–168.
[7] Schalk G, Miller K, Anderson N, et al. Two-dimensional movement control using electrocorticographic signals in humans. J. Neural Eng.. 2008;5(1):75.
[8] Krusienski D, Shih J. Control of a brain–computer interface using stereotactic depth electrodes in and adjacent to the hippocampus. J. Neural Eng.. 2011;8(2):025006.
[9] Shih JJ, Krusienski DJ. Signals from intraventricular depth electrodes can control a brain–computer interface. J Neurosci Methods. 2012;203(2):311–314.
[10] Lachaux J-P, Jerbi K, Bertrand O, et al. BrainTV: a novel approach for online mapping of human brain functions. Biol. Res.. 2007;40(4):401–413.
[11] Jerbi K, Ossandón T, Hamame CM, et al. Task-related gamma-band dynamics from an intracerebral perspective: Review and implications for surface EEG and MEG. Hum. Brain Mapp.. 2009;30(6):1758–1771.
[12] Jerbi K, Freyermuth S, Minotti L, et al. Watching brain TV and playing brain ball: Exploring novel BCI strategies using real-time analysis of human intracranial data. Int Rev Neurobiol. 2009;86:159–168.
[13] Kahane P, Minotti L, Hoffmann D, et al. Invasive EEG in the definition of the seizure onset zone: depth electrodes. Handb Clin Neurol. 2003;3:109–133.
[14] Ghosh S, Laxmi TR, Chattarji S. Functional connectivity from the amygdala to the hippocampus grows stronger after stress. J Neurosci. 2013;33(17):7234–7244.
[15] Oya H, Kawasaki H, Howard MA, et al. Electrophysiological responses in the human amygdala discriminate emotion categories of complex visual stimuli. J Neurosci. 2002;22(21):9502–9512.
[16] Sato W, Kochiyama T, Uono S, et al. Rapid amygdala gamma oscillations in response to fearful facial expressions. Neuropsychologia. 2011;49(4):612–617.
[17] Gaona CM, Sharma M, Freudenburg ZV, et al. Nonuniform high-gamma (60–500 Hz) power changes dissociate cognitive task and anatomy in human cortex. J. Neurosci. 2011;31(6):2091–2100.
[18] Fries P. Neuronal gamma-band synchronization as a fundamental process in cortical computation. Annu Rev Neurosci. 2009;32:209–224.
[19] Fried I, Wilson CL, Maidment NT, et al. Cerebral microdialysis combined with single-neuron and electroencephalographic recording in neurosurgical patients: technical note. J Neurosurg. 1999;91(4):697–705.